A 3D pseudo-spectral method for qP- and qSV- wave simulation in heterogeneous VTI media

Junxiao Li, Huaizhen Chen and Kristopher A. Innanen

ABSTRACT

During reverse time migration in anisotropic media, P- and SV-waves are coupled and the elastic wave equation should be used. However, the crosstalks caused by the interference between different wave modes are detected. Even if an acoustic anisotropic wave equation is used instead, an undesired SV-wave energy could be generated during modeling and reverse time migration. To avoid this unwanted energy, we proposed an approximation of decoupled P-and SV- wave equation system for vertical transversely isotropic (VTI) media. The qP- and qSV- phase velocities for the approximated equations are plotted and compared with the exact and other approximations, which proves its accuracy with different Thomsen parameter sets. The H-PML in second order wavenumber domain is also proposed to eliminate the artificial boundary reflections, comparisons of different absorbing boundary layers are also illustrated to validate the wave number domain H-PML.

INTRODUCTION

Accurate and efficient numerical tools for modelling of seismic wave propagation in reservoir rocks are becoming increasingly indispensable, in research and industry settings, as full-waveform processing and inversion methods increasingly come on line. Representations of rocks with spatially-varying fracture orientations and densities, stress distributions, complex bedding, etc., through anisotropic models, are of particular importance. Under idealized circumstances the SH-mode of the full elastic wavefield propagates independently of the P-SV modes, and can be sensed approximately independently in multicomponent experiments. A first order pseudo-spectral method is proposed to simulate SH wave propagation in VTI medium(Li et al., 2017). Because the computational cost to solve elastic wave equation and the lack of efficient algorithms to compute wave mode separation during migration, the elastic imaging is usually replaced by the acoustic imaging in anisotropic reverse time migration(RTM). However, the qP and qSV wave are usually coupled in anisotropic media. Some cost-effective pseudo-acoustic approaches are thus proposed to anisotropic RTM(Alkhalifah, 1998, 2000). However, undesirable S-wave modes even in the weakly anisotropic regime can be noticed. Because this acoustic approximation sets the shear-wave velocity to zero along the anisotropy symmetry axis, which doesn't mean shear-wave velocity is zero at all directions. Zhou et al. (2006) used a different auxiliary function to decomposed the fourth-order differential equation into a coupled system of second-order differential equations. Bakker and Duveneck (2011) and Zhang et al. (2011) proposed several variations to improve stability and efficiency. But the S-wave artifacts are still present in the wavefield.

The mitigation of the S-wave in the pseudo-acoustic approximation has been an issue since the original work of Alkhalifah (1998). Alkhalifah (2000) pointed out these artifacts can be reduced when the source is located in an isotropic layer, Zhang and Zhang (2009)applied a filter in the wavenumber domain to extract approximate P-wave responses from the pseudo-acoustic simulation so as to reduce the S-wave energy. Alternatively, approximations of the pure acoustic anisotropic wave equations(Du et al., 2007; Etgen and Brandsberg-Dahl, 2009; Crawley et al., 2010; Fowler et al., 2010; Pestana et al., 2011) are also used to suppress the S-wave artifacts. The complete removal of shear-waves can be achieved by factoring out the pure P-wave dispersion relation from the simplified TI P-SV dispersion relation(Liu et al., 2009). Pestana et al. (2012) derive an alternative approximation for the exact factorization which is valid for weak anisotropy and can be implemented using finite difference in time and pseudo-spectral method in space. More sophisticated approximations of this factorization can be found in Du et al. (2013).

Besides the S-wave noise, the periodically extended wavefield on either side of the computational domain caused by the discrete Fourier transform results in numerical contamination of waves. This phenomenon is called wraparound. To avoid this, Fornberg (1996) suggested the Chebyshev PSM be employed, which increases the grid density requirement to π nodes per minimum wavelength. Alternatively, absorbing boundaries (Cerjan et al., 1985), or perfectly matched layers (or PML, Collino and Tsogka, 2001) can also be used to damp the wraparound phases through a gradual reduction of the wavefield amplitude in the vicinity of the grid boundary. Liu (1998) combined the conventional Fourier PSM with perfectly matched layers (PML) to effectively eliminate the wraparound effect. Li et al. (2017) proposed to use the H-PML into first order staggered-grid PSM to simulate SH-wave propagation in heterogeneous VTI media.

In this paper, we first extend the temporal fourth-order PSTD scheme to 3D qP-wavefield simulation in heterogeneous VTI media by using Zhou's eauation(Zhou et al., 2006) and the S-wave energy is still detected. Therefore, a new approximation of the decoupled qP- and qSV-wave equation set is proposed. The comparisons of phase velocities between the new decoupled wave equations and the other approximations are illustrated to validate the precision in different anisotropic medium. The qP- and qSV-wavefield propagation are thus simulated using the new proposed approximations by Fourier pseudo-spectral time-domain PSTD method. A second-order Hybird-PML (Li et al., 2016, 2017) boundary condition is combined with PSTD method to eliminate wraparound effects and boundary reflections. To make comparative conclusions, in this paper, we also implement the H-PML, with a C-PML and M-PML. Finally, qP- and qSV-wave simulation for some numerical models are illustrated.

DECOUPLED WAVE EQUATIONS IN VTI MEDIA

According to Tsvankin (1996), the exact dispersion relation for P and SV waves in VTI media is

$$\frac{v^2(\theta)}{v_{\mathrm{p0}}^2} = 1 + \varepsilon \sin^2\theta - \frac{f}{2} \pm \frac{f}{2}\left[1 + \frac{2\varepsilon\sin^2\theta}{f}\right]\left[1 - \frac{2(\varepsilon-\delta)\sin^2 2\theta}{f(1+\frac{2\varepsilon\sin^2\theta}{f})^2}\right]^{1/2}, \tag{1}$$

where θ is the phase angle measured from the symmetry axis, $v(\theta)$ is the phase velocity of the coupled wave modes; ε and γ are the Thomsen parameters Thomsen (1986):

$$\begin{aligned} \varepsilon &= \frac{c_{11} - c_{33}}{2c_{33}}, \\ \delta &= \frac{(c_{13} + c_{44})^2 - (c_{33} - c_{44})^2}{2c_{33}(c_{33} - c_{44})}, \end{aligned} \tag{2}$$

and $f = 1 - \left(\frac{v_{s0}}{v_{p0}}\right)^2$, where v_{p0} and v_{s0} are the P- and SV-wave velocities $v_{\mathrm{po}} = \sqrt{c_{33}/\rho}$ and $v_{\mathrm{so}} = \sqrt{c_{44}/\rho}$ along the VTI symmetry axis. The plus and minus signs correspond to the P and SV-waves, respectively.

Based on Alkhalifah's approximation, different space/time-domain wave equations have been proposed. If we use the weak anisotropy assumption(Thomsen, 1986), the P-wave and SV-wave phase velocity formula can be simplified by expanding the radical in a Taylor series and dropping the quadratic and higher terms of the anisotropy parameters ε and δ as

$$\begin{aligned} \frac{V_p^2(\theta)}{v_{p0}^2} &= 1 + 2\delta sin^2(\theta)cos^2(\theta) + 2\varepsilon sin^4(\theta), \\ \frac{V_s^2(\theta)}{v_{p0}^2} &= 1 - f + 2(\varepsilon - \delta)sin^2(\theta)cos^2(\theta). \end{aligned} \tag{3}$$

Alkhalifah (2000) obtained the acoustic wave equation for anisotropic VTI media by setting the shear velocity along the symmetry axis to be zero from equation (1), which can be written as

$$\frac{v^2(\theta)}{v_{\mathrm{p0}}^2} = \frac{1}{2} + \varepsilon \sin^2\theta + \frac{1}{2}\sqrt{\left(1 + 2\varepsilon \sin^2\theta\right)^2 - 2(\varepsilon - \delta)sin^2 2\theta}, \tag{4}$$

The dispersion relation for qP waves in 3D acoustic VTI media is thus written as

$$\omega^4 - \left[v_h(k_x^2 + k_y^2) + v_{p0}^2 k_z^2\right]\omega^2 - v_{p0}^2(v_n^2 - v_h^2)(k_x^2 + k_y^2)k_z^2 = 0, \tag{5}$$

where, k_x,k_y and k_z are wavenumbers in the x , y and z directions; ω is angular frequency; v_{p0} is the vertical qP-wave velocity; By setting an auxiliary wavefield function q, Du et al. (2008) derived the pseudo-acoustic wave equations as

$$\begin{aligned} \frac{\partial^2 p}{\partial t^2} &= v_h^2\left(\frac{\partial^2 p}{\partial x^2} + \frac{\partial^2 p}{\partial y^2}\right) + v_{p0}^2\frac{\partial^2 q}{\partial z^2}, \\ \frac{\partial^2 q}{\partial t^2} &= v_n^2\left(\frac{\partial^2 p}{\partial x^2} + \frac{\partial^2 p}{\partial y^2}\right) + v_{p0}^2\frac{\partial^2 q}{\partial z^2}. \end{aligned} \tag{6}$$

The first order SH wave equations are proposed in (Li et al., 2018), which can effectively simulate the wavefield propagation in VTI media. Similarly, by introducing pseudo-velocity components u_p, v_p and w_p of wavefield p and u_q, v_q and w_q of wavefield q based on the split-field technique (Chew and Weedon, 1994; Collino and Tsogka, 2001), the above equation can be further manipulated into

$$\begin{aligned}
&\frac{\partial p}{\partial t} = \rho v_h^2 (\frac{\partial u_p}{\partial x} + \frac{\partial v_p}{\partial y}) + \rho v_{p0}^2 \frac{\partial w_q}{\partial z}, \\
&\frac{\partial q}{\partial t} = \rho v_n^2 (\frac{\partial u_p}{\partial x} + \frac{\partial v_p}{\partial y}) + \rho v_{p0}^2 \frac{\partial w_q}{\partial z}, \\
&\frac{\partial u_p}{\partial t} = \frac{1}{\rho}\frac{\partial p}{\partial x}, \quad \frac{\partial u_q}{\partial t} = \frac{1}{\rho}\frac{\partial q}{\partial x} \\
&\frac{\partial v_p}{\partial t} = \frac{1}{\rho}\frac{\partial p}{\partial y}, \quad \frac{\partial v_q}{\partial t} = \frac{1}{\rho}\frac{\partial q}{\partial y}, \\
&\frac{\partial w_p}{\partial t} = \frac{1}{\rho}\frac{\partial p}{\partial z}, \quad \frac{\partial w_q}{\partial t} = \frac{1}{\rho}\frac{\partial q}{\partial z}.
\end{aligned} \tag{7}$$

However, when we applied the first-order staggered grid PSTD method into the qP-wave simulation, some unwanted energy traveling with a lower speed than the qP-wave can be detected, which is shown in Figure (1). It was pointed out by Grechka et al. (2004) that this unwanted signal is caused by the SV-component, because simply setting $v_s = 0$ does not mean the shear wave phase velocity will vanish in every direction in a VTI medium (Liu et al., 2009). To avoid the undesired SV-wave energy, different approaches have recently been proposed to model the pure P-wave mode.

An easy way is to surround the source with either isotropic or elliptically anisotropic material (Duveneck et al., 2008). In this section, we will formulate a new set of qP and qSV decoupled wave equation set to separate the two wave modes. Instead of setting $V_{s0} = 0$ as Alkhalifah's approximation, we reformulated equation (1) by expanding the square root into the approximations for decoupled P and SV wave phase velocities

$$\begin{aligned}
&\frac{v^2(\theta)}{v_{\mathrm{p0}}^2} \approx 1 + \varepsilon \sin^2\theta + A * F + B * F^2 + O(F^3), \\
&\frac{v^2(\theta)}{v_{\mathrm{p0}}^2} \approx 1 - f + C * F + D * F^2 + O(F^3),
\end{aligned} \tag{8}$$

where,

$$F = \frac{2(\varepsilon - \delta)\sin^2 2\theta}{f(1 + \frac{2\varepsilon \sin^2\theta}{f})^2} \tag{9}$$

A, B and C, D are the first and second order parameters of F after Taylor expansion, respectively (in particular, $A = -\frac{f+2\varepsilon\sin^2\theta}{4}$, $C = \frac{f+2\varepsilon\sin^2\theta}{4}$, $B = -\frac{f+2\varepsilon\sin^2\theta}{16}$, $C =$

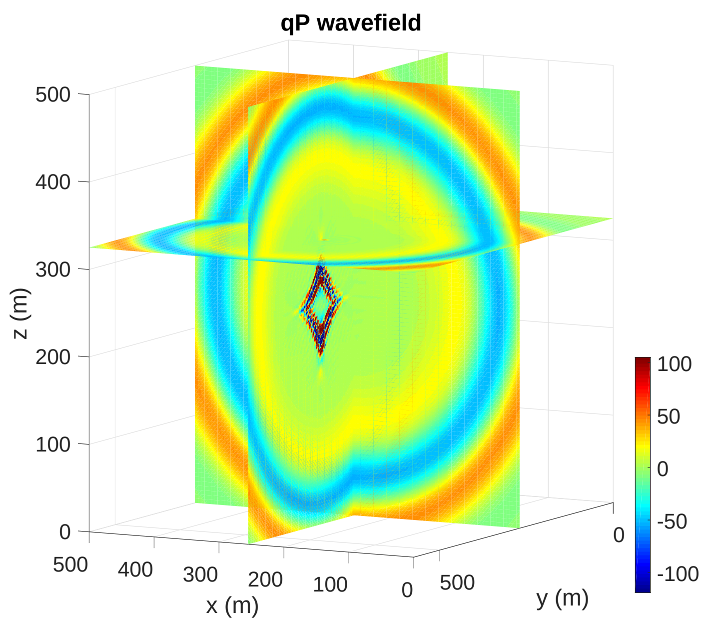

FIG. 1. qP-wave snapshot obtained by the first-order staggered grid PSTD method. The SV-wave energy is detected in the middle of the snapshot.

$\frac{f+2\varepsilon\sin^2\theta}{16}$). $O(F^3)$ are the residuals of the Taylor expansion. We further let $F1 = (\varepsilon - \delta)\sin^2 2\theta$. If we keep the first order term, then the above equations can be further reformulated into

$$\begin{aligned}\frac{v^2(\theta)}{v_{\mathrm{p0}}^2} &= 1 + 2\varepsilon\sin^2\theta + A1 * F1 + O(F^2),\\ \frac{v^2(\theta)}{v_{\mathrm{p0}}^2} &= 1 - f + C1 * F1 + O(F^2),\end{aligned} \tag{10}$$

where, $A1 = -\frac{1}{2(1+\frac{2\varepsilon\sin^2\theta}{f})}$ and $C1 = \frac{1}{2(1+\frac{2\varepsilon\sin^2\theta}{f})}$.

To evaluate the accuracy of the above wave equations, the P-wave phase velocity versus phase angle using $\varepsilon = 0.1, \delta = -0.1$; $\varepsilon = 0.25, \delta = 0.1$; $\varepsilon = 0.4, \delta = 0.1$ and $\varepsilon = 0.4, \delta = 0.25$ are plotted, as shown in Figure 2. Only some slight difference among the curves can be detected. Alkhalifah's formula is closest to the exact solution. The accuracy of the new formula is higher than weak anisotropy approximation while saving considerable computational time compared with the AlkhalifahâĂŹs formula. The above approximations work really well for the P- and SV-wave dispersion relations when $|F \ll 1|$. The qSV-wave phase velocity versus phase angle for different Thomson's parameter sets are also plotted in Figure (3), the comparison with the exact formula and weak formula shows, both the new formula and the weak formula fit the exact formula in weak anisotropic medium (Figure (3)(a)). With the increase of anisotropy, the precision for the new qSV approximation is lower than that of the qP-wave approximated equation, however, the precision of weak formula is the lowest.

Therefore, the above two new equations are to be used for decoupled qP- and qSV-wave simulation. Based on relations $sin\theta = \frac{V(\theta)k_r}{\omega}$ and $cos\theta = \frac{V(\theta)k_z}{\omega}$ with $k_r^2 = k_x^2 + k_y^2$, where ω is the angular frequency, k_x, k_y, k_z are spatial wavenumbers, equation (10) can be expressed as

$$\begin{aligned}\omega^2 &= \left[v_h^2(k_x^2 + k_y^2) + v_{p0}^2 k_z^2\right] + 2A1(v_h^2 - v_n^2)\frac{(k_x^2 + k_y^2)k_z^2}{k_x^2 + k_y^2 + k_z^2} = 0,\\ \omega^2 &= \left[v_{p0}^2(1-f)(k_x^2 + k_y^2 + k_z^2)\right] + 2C1(v_h^2 - v_n^2)\frac{(k_x^2 + k_y^2)k_z^2}{k_x^2 + k_y^2 + k_z^2} = 0.\end{aligned} \tag{11}$$

Multiplying both sides by wavefield $p(\omega, k_x, k_y, k_z)$ in the Fourier domain and followed by an inverse Fourier transform, and using the relation $i\omega \leftrightarrow \frac{\partial}{\partial t}$, the decoupled P wave equation in time-domain is thus derived from equation (11) as

$$\begin{aligned}\frac{\partial^2 p}{\partial t^2} &= \left[v_h^2(\frac{\partial^2}{\partial x^2} + \frac{\partial^2}{\partial y^2}) + v_{p0}^2\frac{\partial^2}{\partial z^2}\right]p - \frac{(v_h^2 - v_n^2)}{1+\varepsilon}(\frac{\partial^2}{\partial x^2} + \frac{\partial^2}{\partial y^2})\frac{\partial^2}{\partial z^2}\frac{p}{\frac{\partial^2}{\partial x^2} + \frac{\partial^2}{\partial y^2} + \frac{\partial^2}{\partial z^2}},\\ \frac{\partial^2 sv}{\partial t^2} &= \left[v_{p0}^2(1-f)(\frac{\partial^2}{\partial x^2} + \frac{\partial^2}{\partial y^2} + \frac{\partial^2}{\partial z^2})\right]sv - 2\frac{(v_h^2 - v_n^2)}{2+\varepsilon}(\frac{\partial^2}{\partial x^2} + \frac{\partial^2}{\partial y^2})\frac{\partial^2}{\partial z^2}\frac{sv}{\frac{\partial^2}{\partial x^2} + \frac{\partial^2}{\partial y^2} + \frac{\partial^2}{\partial z^2}},\end{aligned} \tag{12}$$

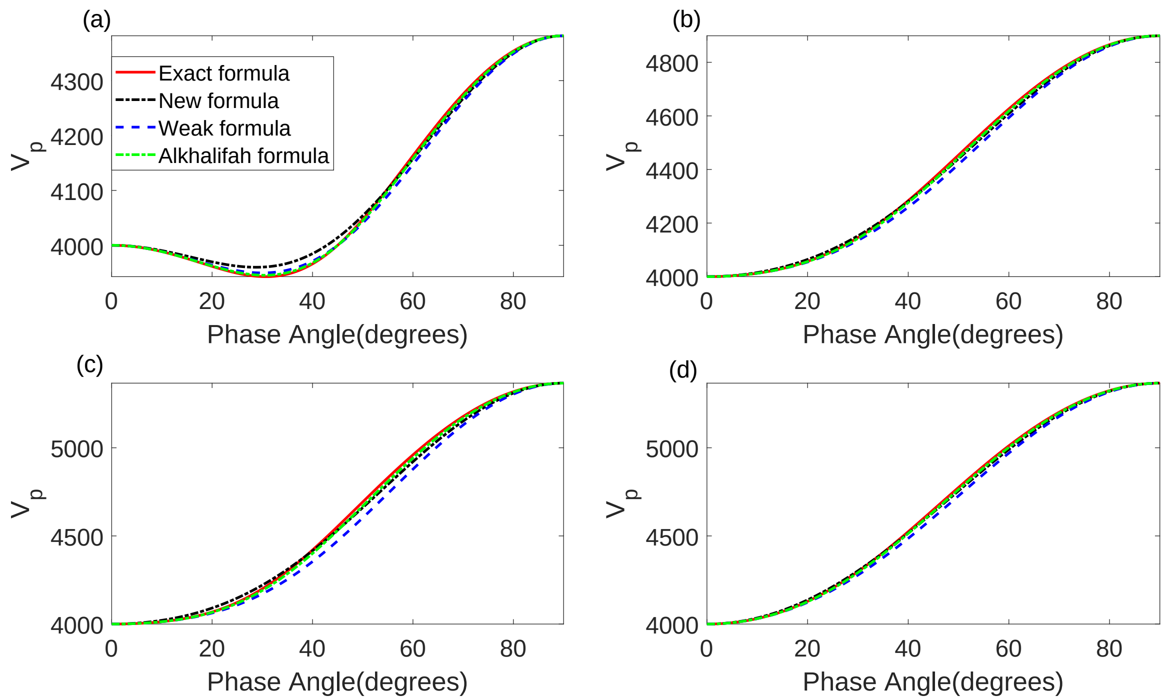

FIG. 2. P-wave phase velocities for a TI medium. In each graph, the green dashed line is the Alkhalifah formula and the dashed blue line plots the P-wave phase velocity using weak formula, the red line is the P-wave phase velocity with exact formula, and the black dashed line corresponds to P-wave phase velocity with the new formula.The qP- and qSV-wave velocities of the medium are 3000m/s and 1500m/s in the direction parallel to the symmetry axis.Different Thomsen parameter sets (a) $\varepsilon = 0.1, \delta = -0.1$; (b) $\varepsilon = 0.25, \delta = 0.1$; (c) $\varepsilon = 0.4, \delta = 0.1$ and (d)$\varepsilon = 0.4, \delta = 0.25$ are used.

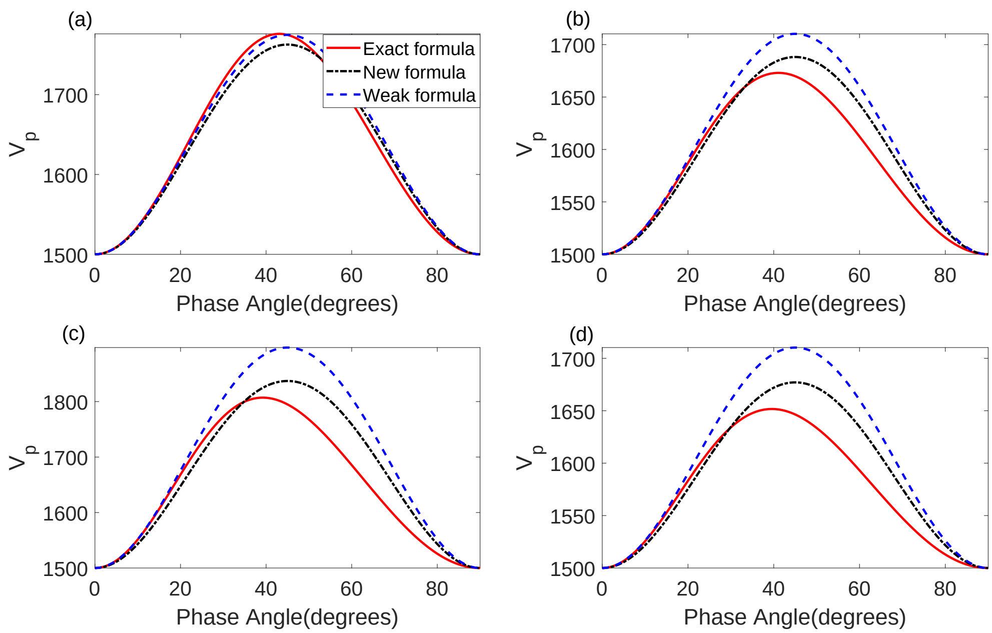

FIG. 3. S-wave phase velocities for a TI medium. In each graph, the dashed blue line plots the P-wave phase velocity using weak formula, the red line is the P-wave phase velocity with exact formula, and the black dashed line corresponds to P-wave phase velocity with the new formula.The qP- and qSV-wave velocities of the medium are 3000m/s and 1500m/s in the direction parallel to the symmetry axis.Different Thomsen parameter sets (a) $\varepsilon = 0.1, \delta = -0.1$; (b) $\varepsilon = 0.25, \delta = 0.1$; (c) $\varepsilon = 0.4, \delta = 0.1$ and (d)$\varepsilon = 0.4, \delta = 0.25$ are used.

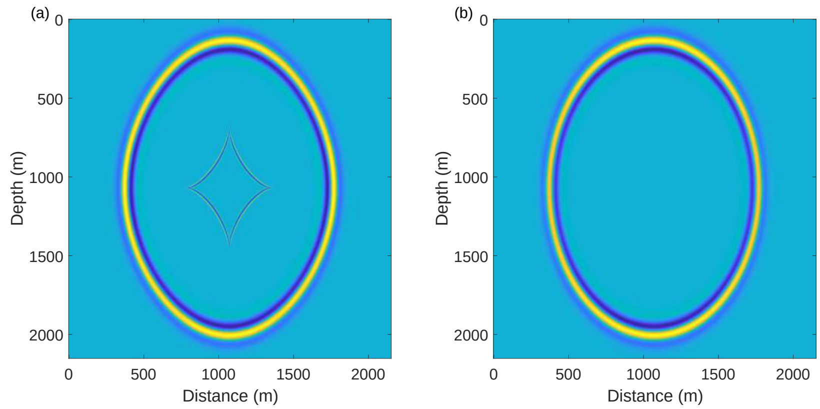

FIG. 4. Snapshots of qP-wave simulation using (a)equation (7) and (b) the new proposed wave equation in a homogeneous VTI medium model. In (a), the SV energy is detected in the middle of the snapshot.

To solve the above equations, we transform the equation set from space-time domain into wave number-time domain as

$$\begin{aligned}
\frac{\partial^2 p}{\partial t^2} &= \left[v_h^2(k_x^2+k_y^2)+v_{p0}^2 k_z^2\right] p - \frac{(v_h^2-v_n^2)}{1+\varepsilon}\left[\frac{(k_x^2+k_y^2)}{k_x^2+k_y^2+k_z^2}\right] k_z^2 p, \\
\frac{\partial^2 sv}{\partial t^2} &= \left[v_{p0}^2(1-f)(k_x^2+k_y^2+k_z^2)\right] sv - 2\frac{(v_h^2-v_n^2)}{2+\varepsilon}\left[\frac{(k_x^2+k_y^2)}{k_x^2+k_y^2+k_z^2}\right] k_z^2 sv,
\end{aligned} \tag{13}$$

We use the pseudospectral method (Fornberg, 1987) that has higher accuracy than lower order finite-difference methods in spatial domain to simulate the wavefield propagation. For the time iteration, a second order center finite difference is applied.

We compare the qP-wave simulation using the above new proposed wave equation with equation (7) in a homogeneous VTI medium model, the snapshots are shown in Figure (4). In Figure (4)(a), the snapshot is simulated by equation (7), in which, the SV energy is detected in the middle of the snapshot. The snapshot shown in Figure (4)(b) is simulated by equation (13), where the pure qP-wave is present without any SV energy.

We also plot the wave comparison at a certain point simulated by the above two equations, which is shown in Figure (5). The waveform in red is simulated by equation (7), compared with the waveform in black simulated by equation (13), the second arrival at about 0.32 s is the SV energy.

SECOND ORDER HPML IN WAVENUMBER DOMAIN

During the forward wavefield modeling, absorbing boundary layers should be added to eliminate artifical boundary reflections when the wavefield propagates to boundaries of a computational model. The hybrid PML (H-PML) method, that combines the advantages of both the C-PML and the M-PML through the optimization of the damping profile, has recently been proposed and proved to be efficient in both isotropic and anisotropic media(Li, et al., 2017). But this method is primarily designed for systems of first-order wave

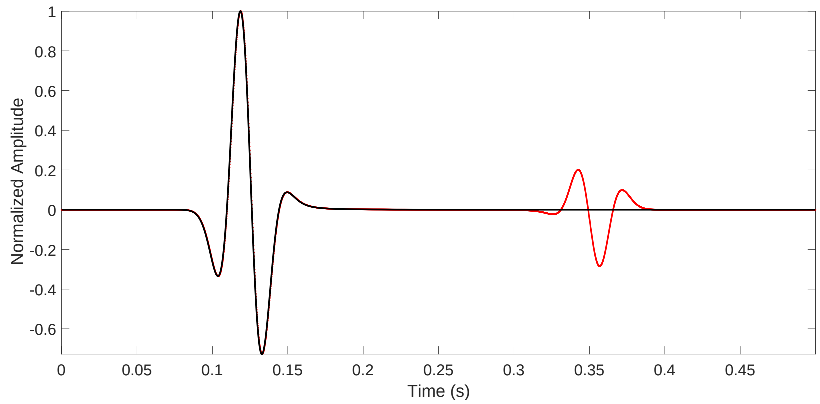

FIG. 5. Wave comparison at a certain point simulated by Zhou's equations(Red) and the new proposed approximation(Black)

equations and cannot be applied directly to second-order systems. Li (Li, et al., 2018, accepted by Pure and applied geophysics) applied the H-PML into the second order in time displacement-stress wave equations, however, the H-PML is still implemented in the first order spacial derivatives of the stress components.

In order to apply the H-PML into the PSTD wave equations with second order spacial derivatives, we start the derivation based on Pasalic and McGarry (2010), in which a detailed derivation of CPML for the second-order acoustic wave equation in space domain are proposed, except the space domain are to be changed into wavenumber domain.

In the H-PML approach, the operators

$$\frac{\partial}{\partial \tilde{x}} = \frac{1}{s_x}\frac{\partial}{\partial x}, \quad \frac{\partial}{\partial \tilde{y}} = \frac{1}{s_y}\frac{\partial}{\partial y}, \quad \text{and} \quad \frac{\partial}{\partial \tilde{z}} = \frac{1}{s_z}\frac{\partial}{\partial z} \tag{14}$$

are introduced. The complex, frequency-shifted, stretched-coordinates s_x, s_y and s_z are

$$\begin{aligned} s_x &= \kappa_x + \tfrac{d_x + m_{x/y} d_y + m_{x/z} d_z}{\alpha_x + i\omega} \\ s_y &= \kappa_y + \tfrac{m_{y/x} d_x + d_y + m_{y/z} d_z}{\alpha_y + i\omega} \\ s_z &= \kappa_z + \tfrac{m_{z/x} d_x + m_{z/y} d_y + d_z}{\alpha_z + i\omega} \end{aligned} , \tag{15}$$

where κ_x, κ_y, and κ_z are real and $\geq$1, and where d_x, d_y, and d_z are damping profiles, ω is the angular frequency and α_x, α_y, and α_z are assumed to be positive and real. The additional damping profiles $m_{i/j}$ for i,j=$(1, 2, 3)$, $i \neq j$, are weighting factors.

In wavenumber domain, the first-order Fourier derivative of a function $u(x)$ can be discretized over a finite grid of N points by Witte and Richards (1990)

$$\mathcal{D}_x u(x_i) = \text{DFT}^{-1}\Bigg[-jk_x \text{DFT}\left[u(x_i)\right]\Bigg], \tag{16}$$

where $j = \sqrt{-1}$, and $x_i = i\Delta x$, and $i = 1, ..., N-1$, with Δx being the sampling interval. The quantity $k_x = 2n\pi/(N\Delta x)$ is the discrete wavenumber in the x direction. For even values of N, n should be chosen as $-N/2 \leq n \leq N/2$, where $n = -N/2$ corresponds to the Nyquist wavenumber. For odd values of N, we choose $-N/2 < n < N/2$. In this case the Nyquist wavenumber does not correspond to one of the grid points. The operators DFT and DFT^{-1} are the forward and inverse discrete Fourier transforms, respectively.

Therefore, equations (14) can be expressed as

$$\begin{aligned}
\mathrm{DFT}^{-1}\Big[-jk_{\tilde{x}}\mathrm{DFT}\Big] &= \tfrac{1}{s_x}\mathrm{DFT}^{-1}\Big[-jk_x\mathrm{DFT}\Big] \\
\mathrm{DFT}^{-1}\Big[-jk_{\tilde{y}}\mathrm{DFT}\Big] &= \tfrac{1}{s_y}\mathrm{DFT}^{-1}\Big[-jk_y\mathrm{DFT}\Big] \\
\mathrm{DFT}^{-1}\Big[-jk_{\tilde{z}}\mathrm{DFT}\Big] &= \tfrac{1}{s_z}\mathrm{DFT}^{-1}\Big[-jk_z\mathrm{DFT}\Big]
\end{aligned} \tag{17}$$

Using the recursive convolution algorithm deduced by Luebbers and Hunsberger (1992), the operator in equation (17) may therefore be written as

$$\begin{aligned}
\mathrm{DFT}^{-1}\Big[-jk_{\tilde{x}}\mathrm{DFT}\Big] &= \tfrac{1}{\kappa_x}\mathrm{DFT}^{-1}\Big[-jk_x\mathrm{DFT}\Big] + \psi_x \\
\mathrm{DFT}^{-1}\Big[-jk_{\tilde{y}}\mathrm{DFT}\Big] &= \tfrac{1}{\kappa_y}\mathrm{DFT}^{-1}\Big[-jk_y\mathrm{DFT}\Big] + \psi_y \\
\mathrm{DFT}^{-1}\Big[-jk_{\tilde{z}}\mathrm{DFT}\Big] &= \tfrac{1}{\kappa_z}\mathrm{DFT}^{-1}\Big[-jk_z\mathrm{DFT}\Big] + \psi_z
\end{aligned} \tag{18}$$

where(we take ψ_x as an example) ψ_x is a memory variable updated at each time step n:

$$\psi_x^n = b_x\psi_x^{n-1} + c_x(\partial_x)^{n-\frac{1}{2}}, \tag{19}$$

in which

$$\begin{aligned}
b_x &= \exp\left[-\left(\frac{d_x + m_{x/y}d_y + m_{x/z}d_z}{\kappa_x + \alpha_x}\right)\triangle t\right] \\
c_x &= \left[\frac{d_x + m_{x/y}d_y + m_{x/z}d_z}{\kappa_x\left(d_x + m_{x/y}d_y + m_{x/z}d_z\right) + \kappa_x\alpha_x}\right](b_x - 1)
\end{aligned}. \tag{20}$$

Introducing new auxiliary variables ϕ_x, ϕ_y, ϕ_z, the second order spatial derivatives in terms of the first-order derivatives can be rewritten as (Pasalic and McGarry, 2010)

$$\mathrm{DFT}^{-1}\Big[(-jk_{\tilde{x}}).^2\mathrm{DFT}\Big] = \tfrac{1}{\kappa_x}\mathrm{DFT}^{-1}\Big[-jk_x\mathrm{DFT}\left(\tfrac{1}{\kappa_x}\mathrm{DFT}^{-1}(-jk_x\mathrm{DFT}) + \psi_x\right)\Big] + \phi_x, \tag{21}$$

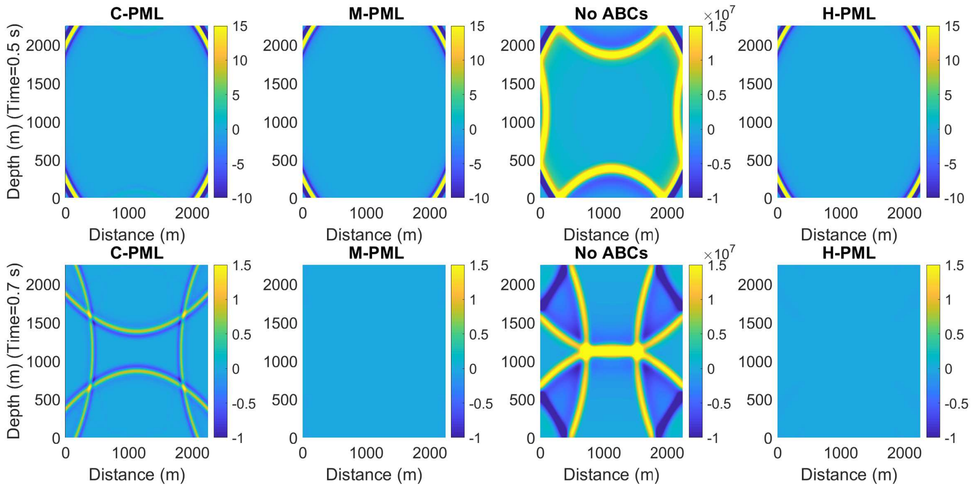

FIG. 6. Snapshots obtained by different boundary conditions at two propagation time. When there is no ABC layers, the boundary reflections are the strongest. The M-PML and H-PML can effectively eliminate the boundary reflections, whereas the C-PML still suffers from boundary reflections.

in wavenumber domain, where

$$\phi_x = b_x \phi_x^{n-1} + c_x \left(\frac{1}{\kappa_x} \mathrm{DFT}^{-1} \left[(-jk_x)^2 \mathrm{DFT} \right]^{(n-\frac{1}{2})} + \frac{\partial \psi_x^{(n-\frac{1}{2})}}{\partial x} \right), \tag{22}$$

We perform a numerical experiment on a VTI medium, whose spatial grid interval is 15m, and the grid number of the physical area is 151×151. The source is a Ricker wavelet with a dominant frequency of 20 Hz. To make a comparison, we compare boundary reflections using different PMLs: the C-PML, M-PML, the new proposed H-PML and no boundary layers. A total number of 15 boundary reflection layers are added at each side of the physical model. Figure (6) shows the snapshots obtained by different boundary conditions at two propagation time. When there is no absorbing boundary condition(ABC) layers, the boundary reflections are the strongest. For the M-PML and C-PML, as is discussed in (Li et al., 2017), the M-PML can effectively eliminate the boundary reflections in VTI media as H-PML, but the C-PML suffers from the boundary reflections, shown in Figure (6).

NUMERICAL EXPERIMENTS

In this section, we present several numerical examples whose purpose is to validate and verify important features of the combination of H-PML and PSM used for qP- and qSV-wave simulation developed in the previous sections.

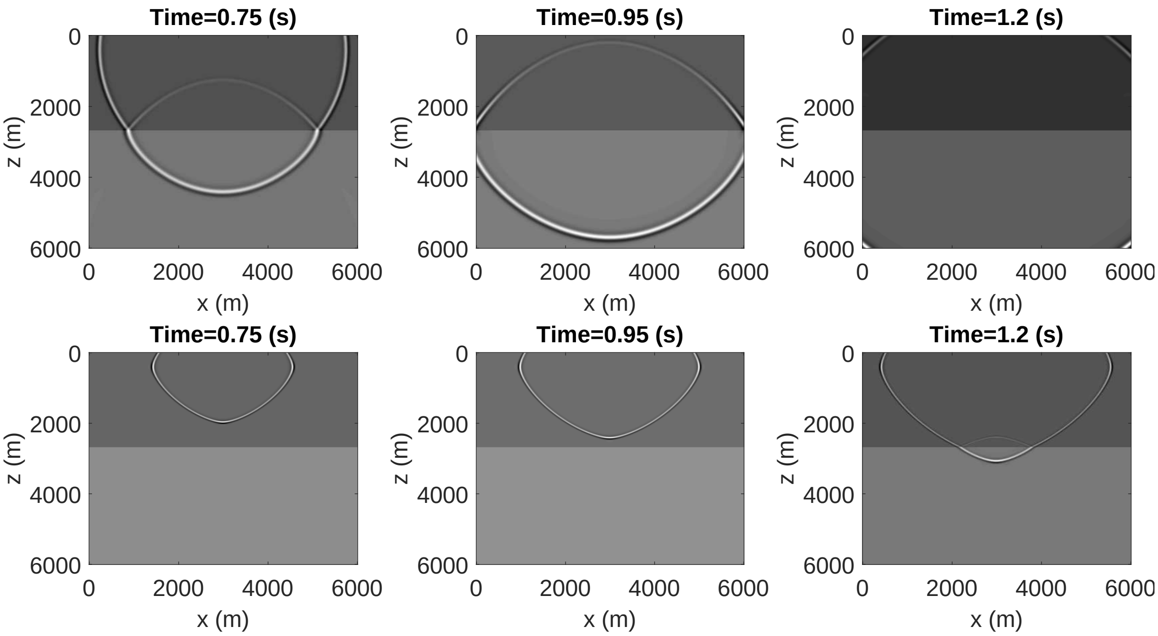

FIG. 7. The normalized qP-(Upper row) and qSV-(lower row) wavefield snapshots for a two-layer model.The qP- and qSV- wave have been separated completely. And the H-PML eliminates the boundary reflections when the wave travels to the boundaries.

Two-layer model

We make use of a two-layer medium to carry out benchmarking. The computational grid is 441×441 with grid spacing $\triangle x = \triangle z = 15m$, including a H-PML of 20 grid points beyond each computational boundary. Waves are initiated with a Ricker wavelet whose central frequency is $f_0 = 20$Hz. We select the time step $\triangle t = 1 \times 10^{-4}s$. The vertical p-wave velocity v_{p0} and sv-wave velocity v_{s0} are $3000m/s, 1700m/s$ and $4000m/s, 2300m/s$ in first and second layer, respectively. The Thomsen parameters ε and δ are $\varepsilon = 0.4, \delta = 0.25$ and $\varepsilon = 0.25, \delta = 0.1$ in first and second layer, respectively. The total simulation time is 1.5s. As is shown in Figure (7), the upper snapshots are the decoupled qP wavefield propagation with the increase of the time; and the lower snapshots are the decoupled qSV wavefield. The qP and qSV-wave are separated completely. When the propagation time is 1.2s, no boundary reflections are detected in the qP-wave snapshot.

In Figure (8), shot gathers of qP- and qSV-wave are also illustrated, respectively. With a total recording time of 1.5s, besides the qP-and qSV-direct waves, the qP-reflection wave is also detected in qP-wave shot gathers. For the qSV-wave, because the velocity is smaller than the qP-wave, no reflection energy is recorded.

Thrust fault model

A heterogeneous anisotropic model with complicated thrust faults is used to examine the stability of the new scheme. The model is $2000m \times 2500m$ with a grid of 400×500.

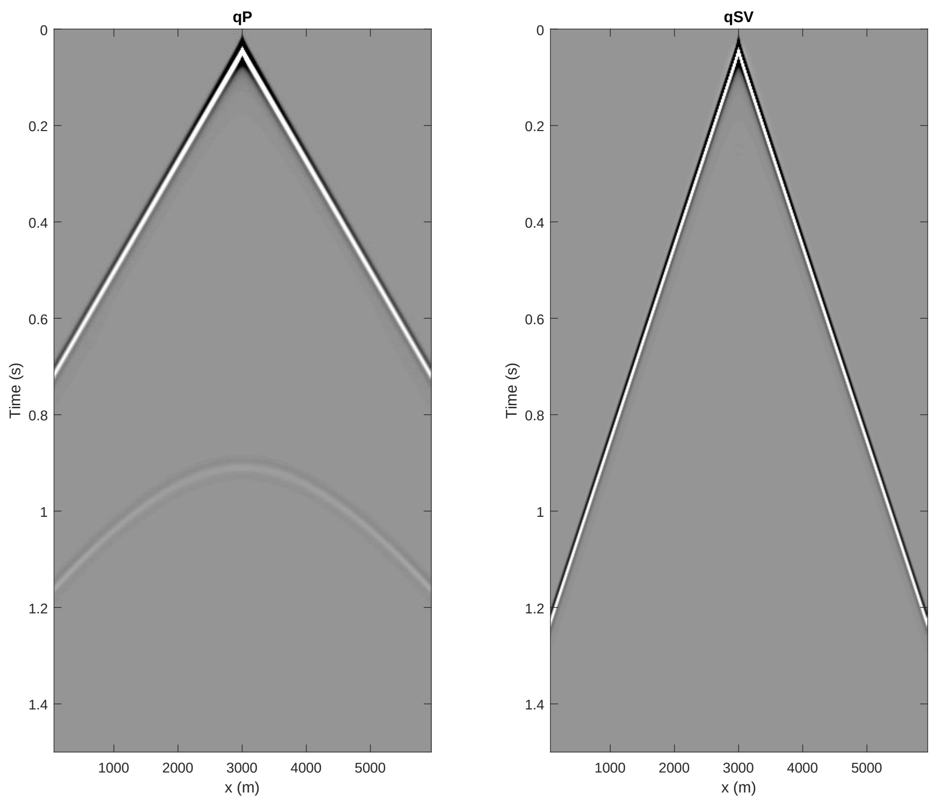

FIG. 8. Shot gathers of qP- and qSV-wave with a total recording time of 1.5s.

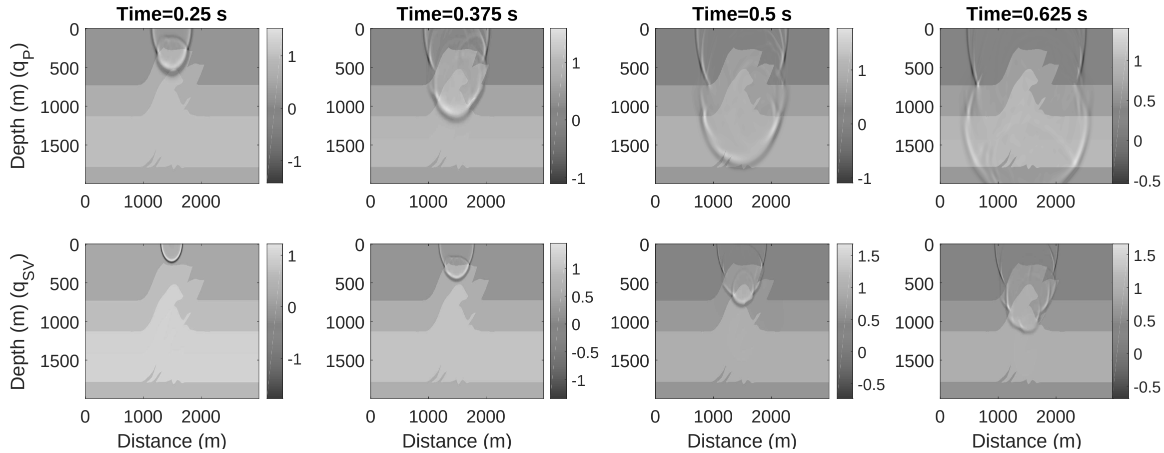

FIG. 9. The normalized qP-(Upper row) and qSV-(lower row) wavefield snapshots.The decoupled qP- and qSV- wave doesn't interfere with each other and no wrap-around, GibbsâĂŹ phenomena are detected

The first layer of the model is isotropic, with P-wave and S-wave velocities at 2400m/s and 1280m/s respectively. The vertical P-wave velocity of the model ranges from 2400 m/s in first layer to 6000 m/s in the bottom layer. The source is located upper middle of the model and emits a Ricker wavelet with dominant frequency of 20Hz. The space and time interval used in this model are 5m and 0.1 ms respectively.

In Figures (9) the normalized qP- and qSV- wavefield snapshots are plotted in the upper and lower planes, respectively. As time evolves, the decoupled qP- and qSV- wave passes from the isotropic regions of the model into the anisotropic layered regions without generating wrap-around errors. No evidence of GibbsâĂŹ phenomena appears. And when the qP wave travels to the boundaries, there is no boundary reflections.

DISCUSSION AND CONCLUSIONS

A new approximation of decoupled qP- and qSV-wave equation set has been proposed, which appears to separate the qP-wave completely from the qSV-wave. The approximated qP- and qSV-phase velocities with different phase angle are illustrated and comapred with some other methods. Compared with equations with higher accurancy, the new equation set doesn't have to deal with the high order wavenumber, which increases the computational cost and the complexity of the wave equations.

In order to eliminate the wrap-around effect and boundary reflections, the H-PML is modified to be applicable for the new decoupled wave equations, which are basically composed of second-order wave number parameters. Numerical comparisons between H-PML, C-PML and M-PML in the second-order wavenumber domain are illustrated and verifies the effectiveness of the H-PML for the new approximation.

Finally, some numerical examples are illustrated, where, the qP- and qSV-wave are separated completely. This new scheme is inspired by previous study on the SH amplitude in borehole environment, a more detailed study on migration and full waveform inversion using this new scheme will be our further work after some benchmarks. Nevertheless, it should also be noticed that the displacement components as well as the velocity component are measured by the new proposed method, which can be directly used for full waveform inversion.

ACKNOWLEDGMENTS

The authors thank the sponsors of CREWES for continued support. This work was funded by CREWES industrial sponsors, NSERC (Natural Science and Engineering Research Council of Canada) through the grant CRDPJ 461179-13, and by the Canada First Research Excellence Fund.

REFERENCES

Alkhalifah, T., 1998, Acoustic approximations for processing in transversely isotropic media: Geophysics, **63**, No. 2, 623–631.

Alkhalifah, T., 2000, An acoustic wave equation for anisotropic media: Geophysics, **65**, No. 4, 1239–1250.

Bakker, P. M., and Duveneck, E., 2011, Stability analysis for acoustic wave propagation in tilted ti media by finite differences: Geophysical Journal International, **185**, No. 2, 911–921.

Cerjan, C., Kosloff, D., Kosloff, R., and Reshef, M., 1985, A nonreflecting boundary condition for discrete acoustic and elastic wave equations: Geophysics, **50**, No. 4, 705–708.

Chew, W. C., and Weedon, W. H., 1994, A 3d perfectly matched medium from modified maxwell's equations with stretched coordinates: Microwave and optical technology letters, **7**, No. 13, 599–604.

Collino, F., and Tsogka, C., 2001, Application of the perfectly matched absorbing layer model to the linear elastodynamic problem in anisotropic heterogeneous media: Geophysics, **66**, No. 1, 294–307.

Crawley, S., Brandsberg-Dahl, S., McClean, J., and Chemingui, N., 2010, Tti reverse time migration using the pseudo-analytic method: The Leading Edge, **29**, No. 11, 1378–1384.

Du, X., Bancroft, J. C., and Lines, L. R., 2007, Anisotropic reverse-time migration for tilted ti media: Geophysical Prospecting, **55**, No. 6, 853–869.

Du, X., Fletcher, R., and Fowler, P., 2008, A new pseudo-acoustic wave equation for vti media, *in* 70th EAGE Conference and Exhibition incorporating SPE EUROPEC 2008.

Du, X., Fowler, P. J., and Fletcher, R. P., 2013, Recursive integral time-extrapolation methods for waves: A comparative review: Geophysics, **79**, No. 1, T9–T26.

Duveneck, E., Milcik, P., Bakker, P. M., and Perkins, C., 2008, Acoustic vti wave equations and their application for anisotropic reverse-time migration, *in* SEG Technical Program Expanded Abstracts 2008, Society of Exploration Geophysicists, 2186–2190.

Etgen, J. T., and Brandsberg-Dahl, S., 2009, The pseudo-analytical method: Application of pseudo-laplacians to acoustic and acoustic anisotropic wave propagation, *in* SEG Technical Program Expanded Abstracts 2009, Society of Exploration Geophysicists, 2552–2556.

Fornberg, B., 1987, The pseudospectral method: Comparisons with finite differences for the elastic wave equation: Geophysics, **52**, No. 4, 483–501.

Fornberg, B., 1996, A practical guide to pseudospectral methods, vol. 1 of cambridge monographs on applied and computational mathematics.

Fowler, P. J., Du, X., and Fletcher, R. P., 2010, Coupled equations for reverse time migration in transversely isotropic media: Geophysics, **75**, No. 1, S11–S22.

Grechka, V., Zhang, L., and Rector III, J. W., 2004, Shear waves in acoustic anisotropic media: Geophysics, **69**, No. 2, 576–582.

Li, J., Innanen, K., Lines, L., and Tao, G., 2016, Wavefield simulation of 3d borehole dipole radiation, *in* SEG Technical Program Expanded Abstracts 2016, Society of Exploration Geophysicists, 744–748.

Li, J., Innanen, K. A., and Tao, G., 2018, A 3d pseudo-spectral method for sh wave simulation in heterogeneous media, *in* SEG Technical Program Expanded Abstracts 2018, Society of Exploration Geophysicists, 4005–4009.

Li, J., Innanen, K. A., Tao, G., Zhang, K., and Lines, L., 2017, Wavefield simulation of 3d borehole dipole radiation: Geophysics, **82**, No. 3, D155–D169.

Liu, F., Morton, S. A., Jiang, S., Ni, L., and Leveille, J. P., 2009, Decoupled wave equations for p and sv waves in an acoustic vti media, *in* SEG Technical Program Expanded Abstracts 2009, Society of Exploration Geophysicists, 2844–2848.

Liu, Q. H., 1998, The pseudospectral time-domain (pstd) algorithm for acoustic waves in absorptive media: IEEE transactions on ultrasonics, ferroelectrics, and frequency control, **45**, No. 4, 1044–1055.

Luebbers, R. J., and Hunsberger, F., 1992, Fdtd for nth-order dispersive media: IEEE transactions on Antennas and Propagation, **40**, No. 11, 1297–1301.

Pasalic, D., and McGarry, R., 2010, Convolutional perfectly matched layer for isotropic and anisotropic acoustic wave equations, *in* SEG Technical Program Expanded Abstracts 2010, Society of Exploration Geophysicists, 2925–2929.

Pestana, R. C., Ursin, B., and Stoffa, P. L., 2011, Separate p-and sv-wave equations for vti media, *in* SEG Technical Program Expanded Abstracts 2011, Society of Exploration Geophysicists, 163–167.

Pestana, R. C., Ursin, B., and Stoffa, P. L., 2012, Rapid expansion and pseudo spectral implementation for reverse time migration in vti media: Journal of Geophysics and Engineering, **9**, No. 3, 291.

Thomsen, L., 1986, Weak elastic anisotropy: Geophysics, **51**, No. 10, 1954–1966.

Tsvankin, I., 1996, P-wave signatures and notation for transversely isotropic media: An overview: Geophysics, **61**, No. 2, 467–483.

Witte, D., and Richards, P., 1990, Computational acoustics.

Zhang, Y., and Zhang, G., 2009, One-step extrapolation method for reverse time migration: Geophysics, **74**, No. 4, A29–A33.

Zhang, Y., Zhang, H., and Zhang, G., 2011, A stable tti reverse time migration and its implementation: Geophysics, **76**, No. 3, WA3–WA11.

Zhou, H., Zhang, G., and Bloor, R., 2006, An anisotropic acoustic wave equation for vti media, *in* 68th EAGE Conference and Exhibition incorporating SPE EUROPEC 2006.